On the Mechanical and Thermal Properties of Poly(Vinyl Alcohol) – Alginate Composite Yarn Reinforced with Nanocellulose from Oil Palm Empty Fruit Bunches

Ainul Maghfirah[1], Farah Fahma[2*], Nurmalisa Lisdayana[3], Muchammad Yunus[4], Ahmad Kusumaatmaja[5], and Grandprix Thomryes Marth Kadja[6,7,8]**

[1]*Department of Applied Chemistry, Graduate School of Engineering, Kyushu University, 744 Motooka, Nishi-ku, Fukuoka 819-0395, Japan*

[2]*Department of Agroindustrial Technology, Faculty of Agricultural Engineering and Technology, Bogor Agricultural University, Gedung Fateta, Jl. Raya Dramaga, Kampus IPB Dramaga, Bogor 16680, West Java, Indonesia*

[3]*Department of Agroindustrial Technology, Institut Teknologi Sumatera, Jl. Terusan Ryacudu, Way Hui Jati Agung, South Lampung 35365, Indonesia*

[4]*Department of Veterinary Parasitology, Faculty of Veterinary Medicine, Airlangga University, Campus C, Jl. Mulyorejo, Surabaya 60115, Indonesia*

[5]*Department of Physics, Faculty of Mathematics and Natural Sciences, Universitas Gadjah Mada, Sekip Utara, Yogyakarta 55281, Indonesia*

[6]*Division of Inorganic and Physical Chemistry, Faculty of Mathematics and Natural Sciences, Institut Teknologi Bandung, Jl. Ganesha No. 10, Bandung 40132, Indonesia*

[7]*Research Center for Nanosciences and Nanotechnology, Institut Teknologi Bandung, Jl. Ganesha No. 10, Bandung 40132, Indonesia*

[8]*Center for Catalysis and Reaction Engineering, Institut Teknologi Bandung, Jl. Ganesha No. 10, Bandung 40132, Indonesia*

Corresponding author:

email: farah_fahma@apps.ipb.ac.id[*]; kadja@chem.itb.ac.id[**]

Received: July 24, 2021
Accepted: October 25, 2021

DOI: 10.22146/ijc.67881

Abstract: *PVA-alginate hydrogel is a promising material for use in biomedical applications due to its desirable characteristics: biocompatible, durable, non-toxic, and low cost. However, the low gel strength of this composite limits its use in biomedical applications. This study aims to develop enhanced mechanical and thermal properties of poly(vinyl alcohol) PVA-alginate composite yarn by adding nanocellulose isolated from the sustainable oil palm empty fruit bunches (OPEFBs). The PVA-alginate composite yarns reinforced with nanocellulose were prepared with various nanocellulose contents (1 wt.%, 2 wt.%, and 5 wt.%). The composite's tensile strength exhibited an increasing trend with the addition of nanocellulose, while the elongation at break showed the opposite trend. Moreover, it was demonstrated that the composite's thermal degradation shifts to higher temperatures with the addition of nanocellulose. The observed activation energies for the thermal degradation calculated using the Coats-Redfern method exhibited a significant increment for the composites reinforced with nanocellulose. These results show that the addition of nanocellulose into the PVA-alginate matrix enhances the chemical and thermal properties of the resulting hydrogel. All these improvements have resulted from more abundant and robust hydrogen bonds generated by the nanocellulose presence.*

Keywords: *nanocellulose; OPEFBs; PVA-alginate; mechanical stability; thermal stability*

■ INTRODUCTION

Recently, the utilization of sustainable resources to produce new biodegradable materials has been intensively pursued as an alternative to the continuously declining raw material from non-renewable resources. In this sense, palm oil has emerged as one of the most potent

resources. From 1962 to 2012, palm oil plantation across the globe has expanded exponentially to around 13 million hectares establishing them as the global fastest-growing monoculture [1-2]. Indonesia is the largest palm-oil producing country globally, with a national annual yield of 17 tons of fresh fruit bunches per hectare [3]. However, the massive production is surely followed by a large number of wastes. The waste in palm oil plantations is dominated by biomass, such as oil palm empty fruit bunches (OPEFBs), fronds, trunks, and mesocarps. For example, OPEFBs are the solid-waste biomass produced after the stripping process of fresh fruit bunches. OPEFBs are composed of crystalline cellulose (41.3–46.5%), which is embedded in an amorphous matrix of lignin (27.6–32.5%) and hemicellulose (25.3–33.8%) [4].

Nowadays, many researchers have focused on the use and recycling of OPEFBs because of their exceptional potential as an organic carbon source and sustainability in producing high value-added materials, such as activated carbon [5-8], bioethanol [9-12], and nanocellulose [13-16]. Among them, nanocellulose has been an up-and-coming class of materials, which has a broad spectrum of applications, including food packaging [17], tissue engineering [18], pharmaceutics [19], and wound treatment [20-21]. These are possible due to their high surface area, hydrophilicity, mechanical strength, biocompatibility, biodegradability, and lack of toxicity. It becomes more interesting with the strong artificial adhesion and dispersion capability of nanocellulose in various host materials/matrices, leading to the potential use as reinforcement in polymer composite materials [13,15,22].

Many polymers have been studied as a system to be reinforced with nanocellulose, e.g., polyvinyl alcohol (PVA) [23], polyacrylamide [24], chitosan [25], and alginate [26]. These reports have shown the increased higher mechanical properties of the system after the incorporation of nanocellulose. Moreover, Poonguzhali et al. [27] reported that nanocellulose incorporation up to 10% into chitosan/poly(vinyl pyrrolidone) matrix improved wound healing yarn with a tensile strength of 39.7 ± 6.9 MPa. Similar nanocellulose reinforcements in various blend polymers have also been demonstrated [13,15,28]. In addition, Li et al. [29] also found that adding a small amount of long filamentous nanocellulose fibrils (NCFs) into PVA films increased the maximum degradation temperature around 4 to 16.9 °C indicating that nanocellulose addition also could enhance the thermal stability of the PVA films.

PVA-alginate is a hydrogel system that has attracted much attention, especially for its biomedical application. However, as it is highly hydrophilic, the mechanical strength is usually low, limiting its use in certain applications. Therefore, many efforts have been devoted to improving the properties of the PVA-based composite system. For example, by immersing PVA-alginate composite in the saturated NaCl aqueous solution, Jiang et al. [30] produced PVA-alginate with an improved mechanical strength (maximum tensile strength of 1.34 MPa). On the other hand, Islam and Karim [31] also reported a better tensile property of PVA-alginate blend nanofiber up to 35 MPa using the electrospinning method. Meanwhile, cross-linking PVA and sodium alginate using glutaraldehyde and calcium sulfate with the presence of nanocellulose showed compressive stress of up to 79.5 ± 2.35 kPa, which was 3.2 times higher than the pristine PVA/alginate hydrogel.

Herein, we report the preparation of PVA-alginate nanocomposite yarn modified with nanocellulose isolated from OPEFBs. The thermal stability of PVA-alginate with various nanocellulose content is investigated in detail resulting in the observed activation energies for their decomposition. Moreover, the tensile strength of PVA-alginate-nanocellulose yarn is thoroughly studied at different temperatures. Finally, the improved mechanical and thermal stabilities are correlated to the interaction between nanocellulose and PVA-alginate systems. Our results may provide valuable insights into the versatile design of polymer systems reinforced with nanocellulose.

■ EXPERIMENTAL SECTION

Materials

The fibers of OPEFBs for the production of nanocellulose were obtained from PTPN VIII, Kertajaya, Lebak, West Java, Indonesia. PVA (Celvol TM Sekisui Chemical Co., Ltd, Jakarta, Indonesia), sodium hydroxide

(NaOH, Merck), and hydrogen peroxide (H_2O_2, Merck) used were the commercial-grade products. All chemicals were used as received without further purification.

Instrumentation

X-ray diffraction (XRD) patterns were collected on a Bruker D8 Advance diffractometer using a Cu-Kα radiation beam (λ = 1.54 Å) from 2θ of 3° to 50° with a step size of 0.02°. The samples were placed on a 3 cm-diameter sample holder, and the measurement started under operating conditions of 40 kV and 40 mA. The morphologies of the materials were observed on a Hitachi SU-3500 scanning electron microscope (SEM) with a secondary electron (SE) mode at an accelerating voltage of 10 kV. The isolated nanocellulose was observed on a JEOL JEM 1010 transmission electron microscope (TEM). A Shimadzu Prestige spectrometer was employed to record the Fourier-transform infrared (FTIR) spectra of the samples with a spectral resolution of 4 cm^{-1}. Each spectrum was resulted from 64 scans. The thermal properties of the samples were analyzed using a Hitachi simultaneous thermal analyzer (STA) 7000 using N_2 (80 vol%) and O_2 (20 vol%) as the carrier gas with a flow rate of 50 mL min^{-1}. The temperature was increased to 600 °C at a fixed heating rate of 20 °C min^{-1}. The mechanical properties of the samples were analyzed using a Universal Testing Machine (Instron 3369) at a rate of 6 mm min^{-1}. Five measurements were carried out for each sample.

Procedure

Isolation of cellulose fibers from OPEFBs

The dried OPEFBs fibers were soaked in a 10 wt.% NaOH solution with a ratio of solution/fibers = 20/1 (v/w) at 95 °C for 1 h. In this step, the black solution was resulted due to the leaching of lignin. Subsequently, the fibers were separated from the black solution, washed, and filtered using distilled water until the neutral filtrate pH. After that, the obtained fibers were dried at 55 °C for 24 h. Furthermore, the bleaching was performed by immersing the delignified OPEFBs in 30 wt.% hydrogen peroxide solution with a solution/fibers ratio of 15/1 (v/w) at 95 °C for 1.5 h. The cellulose fibers were filtered and washed to neutral. The second stage of bleaching was performed using alkaline peroxide solution, obtained by mixing 30 wt.% H_2O_2 and 10 wt.% NaOH solutions, with a volume ratio of 2/1. The cellulose fibers were then immersed in this solution with a solution/fibers ratio of 15/1 (v/w) at 95 °C for 1.5 h. The cellulose fibers were filtered and washed to neutral. After the two-step bleaching treatment, the white cellulose fibers are obtained.

Isolation of nanocellulose from cellulose fibers

The cellulose fibers were diluted using distilled water to a concentration of 2 wt.%. Subsequently, the mixture was treated with an ultrafine grinder (Masuko Co., Ltd, Kawaguchi, Japan) at 1500 rpm with several gap levels, i.e., +5 (15 times), 0 (15 times), –5 (15 times), –10 (15 times), –15 (15 times) and –18 (15 times) [32], performed gradually. After the ultrafine grinding, a thick suspension was obtained and mixed with distilled water with a suspension/water ratio of 1:2 (v/v). Finally, the mixture underwent ultrasonication treatment ((20 kHz, 40 W, Q Sonica, Newtown, CT, USA) for 1 h to produce nanocellulose.

Production of nanocellulose composite yarn by wet spinning

The nanocellulose was dispersed in distilled water, followed by the addition of sodium alginate under stirring for 40 min under vigorous stirring. Subsequently, PVA was added, and the stirring was continued for 40 min at 200 °C. The final mixture has a PVA/alginate weight ratio of 1/1 and the PVA-alginate-nanocellulose to water weight ratio of 25. The content nanocellulose was varied, i.e., 0 wt.%, 1 wt.%, 2 wt.%, and 5 wt.%, relative to the total weight of PVA-alginate-nanocellulose. Then, the mixture was subsequently spun using a 2.5 mm needle with a spinning speed of 20 mL min^{-1}. The dope was coagulated in a 9 wt.% $CaCl_2$ solution followed by washing with distilled water. The resulting filament was then dried at room temperature for 4–6 h followed by soaking in distilled water for 15 min and dried in the oven at 55 °C for 30 min.

■ RESULTS AND DISCUSSION

The Structural Properties

Fig. 1 shows the TEM image of the isolated nanocellulose from the OPEFBs. The isolated nanocellulose exhibits thin, dendritic fibrous morphology

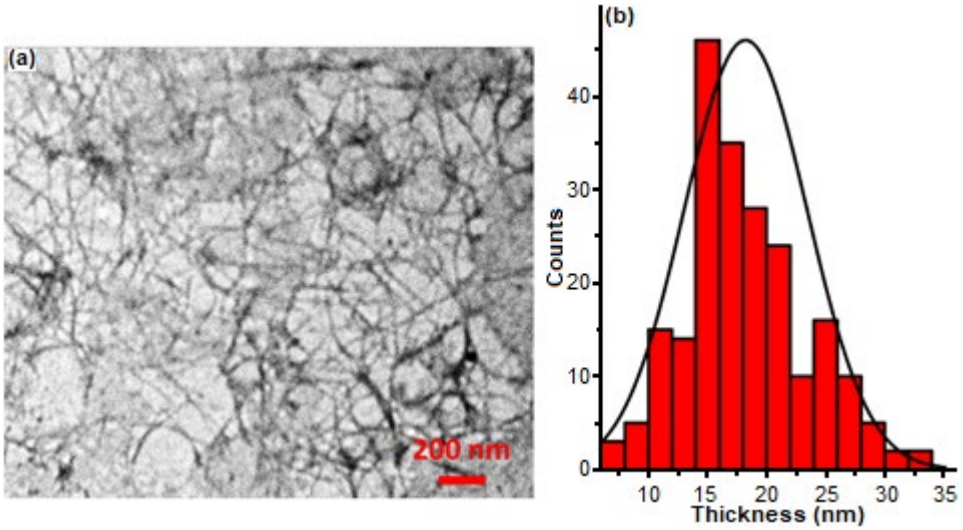

Fig 1. (a) TEM image and (b) the corresponding thickness distribution of the nanocellulose isolated from OPEFBs

with single and connected frameworks of filaments. This characteristic morphology of nanocellulose was rendered from strong hydrogen bonds amount the filaments [33]. The thickness distribution of the isolated nanocellulose is centered at around 20 nm, as depicted in Fig. 1(b).

The XRD patterns of all studied materials are shown in Fig. 2. All materials exhibit a dominant peak at 2θ of 19.6°, attributed to the strong intermolecular and intramolecular hydrogen bonding within the PVA structure [13,31]. No other peaks appear at 2θ of 13.7° and 23° [34], which should belong to the alginate structure. It indicates that the alginate structure might be distorted due to hydrogen bonding interaction between hydroxyl (–OH) and carbonyl (C=O) groups of alginate with hydroxyl groups of PVA. Meanwhile, the characteristic peak of nanocellulose appeared at 2θ of 22.5°, corresponding to cellulose's (200) crystal plane [35-36] with the PVA-alginate structure. The intensity of this peak increases along with the addition of nanocellulose. This result shows that the nanocellulose is successfully incorporated into the PVA-alginate composite structure. The nanocellulose addition up to 5 wt.% does not disturb the structure of the PVA-alginate composite. Moreover, a slight increase of crystallinity was observed with nanocellulose addition up to 2 wt.%. These results are similar to the work performed by Uddin et al. [37], where the addition of a small amount of cellulose whisker (CW) into PVA increased the degree of crystallinity of the fiber,

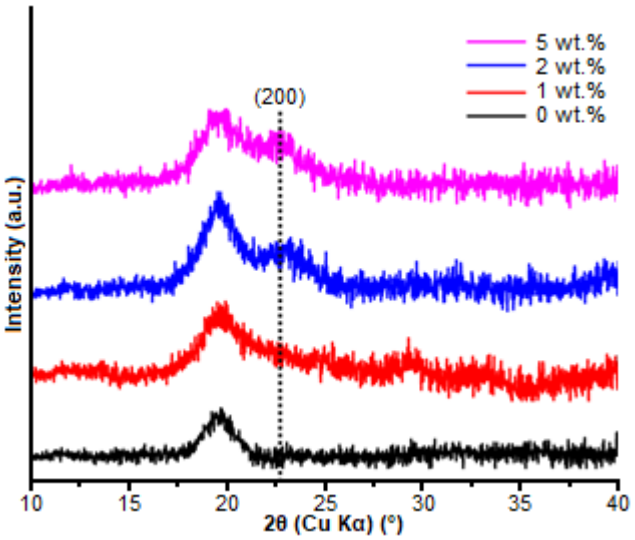

Fig 2. XRD patterns of PVA-alginate composites with different amounts of nanocellulose addition

while a higher concentration of CW, the ratio of CW and PVA weight > 5%, resulted in a lower degree of crystallinity. It was confirmed by wide-angle X-ray diffraction (WAXD) analysis that PVA-CW composite with CW/PVA weight ratio of 5% showed more enhanced crystal orientation of PVA component. Thus, the broader peak at 19.6° of PVA-alginate with 5 wt.% addition of nanocellulose is probably due to the impeded orientation of the PVA component caused by a large amount of nanocellulose network [15,38].

The effect of nanocellulose addition on the structural change and the molecular interaction was

further analyzed using FTIR spectroscopy, as depicted in Fig. 3. The vibrational bands at around 1418 and 1630 cm^{-1} are assigned to symmetric and asymmetric stretching of $–COO^-$ from alginate, respectively, [31], while bands at around 2920 cm^{-1} correspond to C–H asymmetric stretching from the alkyl group [39]. In addition, the hydroxyl (O–H) group is shown by the broadband centered at around 3448 cm^{-1}. This peak is attributed to all types of hydrogens bonded to hydroxyl groups. Furthermore, with the addition of nanocellulose, the O–H stretching vibration band undergoes a redshift to the lower wavenumber (Fig. 3(c)). This trend correlates to the stronger hydrogen bond within the composite with the addition of nanocellulose. The relationship between hydrogen bond strength and the stretching vibration redshift has been discussed in previous publications [40-41]. The added nanocellulose may likely penetrate between PVA and alginate backbones; thus, resulting in stronger interaction through hydrogen bonds. The molecular interactions of the present PVA-alginate composites yarn reinforced with nanocellulose are schematically illustrated in Fig. 4. The alginates form ionically cross-linking interactions to Ca-dicarboxylate chelate triplets since the composites were immersed in $CaCl_2$ solution during the preparation. Meanwhile, hydrogen bonds arise from hydroxyl bonds in PVA and nanocellulose.

The Morphological Analysis

Fig. 5 displays SEM images of PVA-alginate composite yarn with various amounts of nanocellulose at the same magnification and their corresponding 3D surface reconstruction. The morphology of the PVA-alginate composite without the addition of nanocellulose shows a relatively smooth surface with several folds (Fig. 5(a)). Nevertheless, some tears are observed as indicated by red arrows in Fig. 5(a), which might be due to the relatively weak interaction. On the other hand, tears do not appear in the samples with the

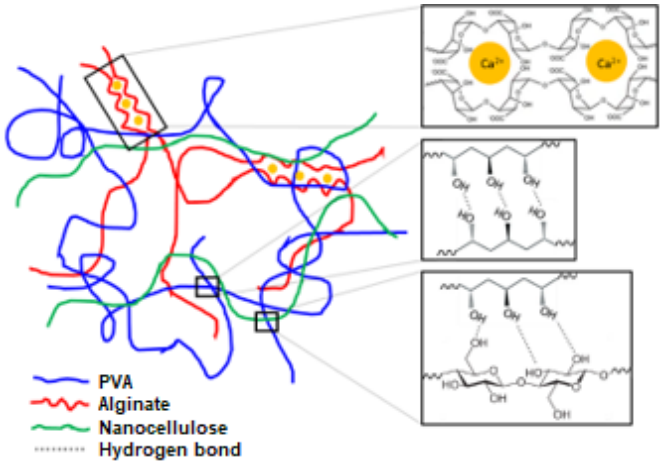

Fig 4. Schematic illustration of molecular interactions within PVA-alginate composites reinforced with nanocellulose

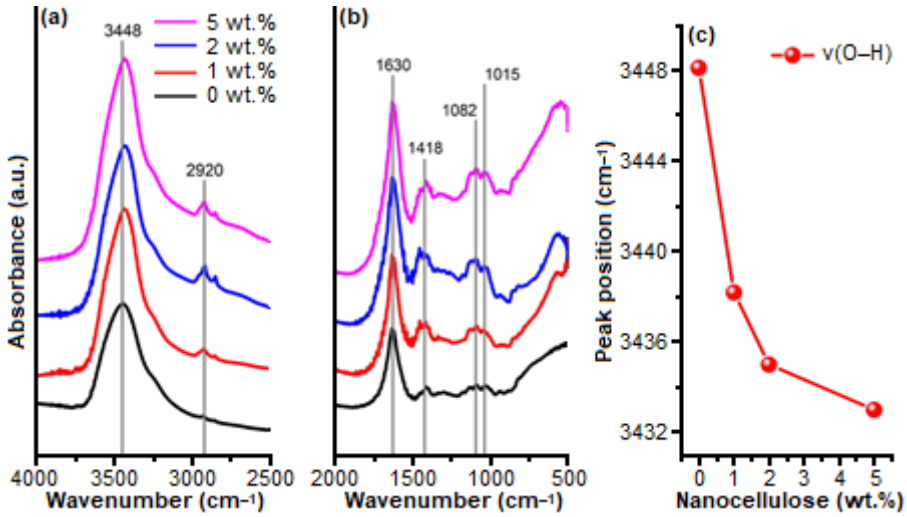

Fig 3. (a, b) FTIR spectra of PVA-alginate composites with different amounts of nanocellulose addition, and (c) the shift of O–H stretching vibration position as a function of nanocellulose addition

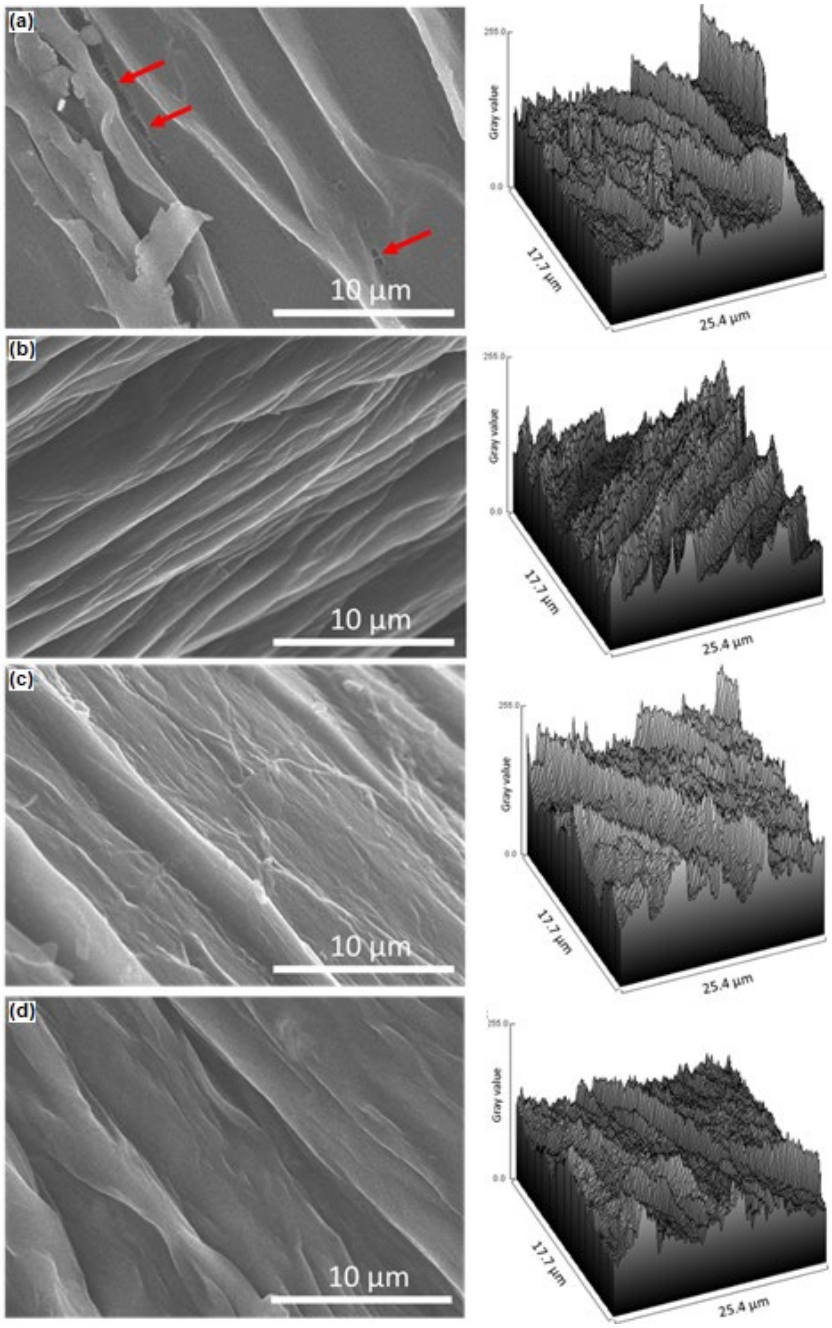

Fig 5. SEM images of PVA-alginate composites with nanocellulose addition of (a) 0 wt.% (b) 1 wt.%, (c) 2 wt.%, and (d) 5 wt.%

presence of nanocellulose. The addition of nanocellulose somewhat alters the surface morphology of the composite into rougher and filamentous, as also indicated by 3D surface construction. These observations are likely to be generated by the presence of nanocellulose. It appears that the nanocellulose is well-dispersed and a compatible nanofiller to the polymer matrices.

The Mechanical Properties

The tensile strength and elongation at break of PVA-alginate composites with different nanocellulose content are provided in Fig. 6. As more cellulose is added to the PVA–alginate, the tensile strength is enhanced. This phenomenon is associated with the effective

interfacial adhesion of PVA-alginate matrices with nanocellulose generated by the more and stronger hydrogen bonds. Li et al. [42] reported that the tensile strength of PVA-alginate hydrogels resulted from the ionically cross-linked structure of alginate due to the immersion ion $CaCl_2$ aqueous solution the hydrogen bonds among PVA networks. The former was broken upon initial stretched while the latter survived more stress, which shows the significant contribution of hydrogen bonds to the mechanical properties of the polymer matrices. The elongation at break tends to decline with the increase of nanocellulose content since nanocellulose can raise the stiffness effect originated from the more rigid structures due to the more abundant and robust hydrogen bond. Interestingly, a sharp decrease of elongation at break was observed at nanocellulose of 1 wt.%. It is probably because of the weak interaction between nanocellulose and the PVA-alginate matrix. However, this hypothesis merits further investigation. Our results agree with the work performed by Cho and Park [43]. They reported that the tensile modulus and strength of PVA nanocomposite were enhanced with the nanocellulose addition. Their nanocellulose was extracted from the microcrystalline cellulose through sulfuric acid hydrolysis. Similar trends of tensile strength and elongation at break to our study were reported by El Miri et al. [44] for carboxymethyl cellulose–starch composite reinforced with nanocellulose.

The Thermal Properties

The thermal properties of all studied materials are assessed using thermogravimetric analysis (TGA) and shown in Fig. 7(a). As the temperature increases, the mass of the samples decreases. This fact indicates the conversion, α, according to the following equation,

$$\alpha = \frac{m_o - m_t}{m_o - m_f} \quad (1)$$

where m_o and m_f are the initial and final mass of the samples, respectively, while m_t is the mass of the samples at a certain time, t. The initial stage is observed from around 50 to 200 °C, attributed to the evaporation of water molecules. Above 200 °C, the conversion increases dramatically, which can be classified into several stages, as shown by the first derivative of the thermogravimetric curve (Fig. 7(b)). Around 230 to 330 °C, the conversion is due to the dehydration and the formation of polyene. Moreover, a more intense conversion occurs from around 330 to 420 °C attributed to the polyene decomposition resulting in oxygen-containing molecules. Holland and Hay reported [45] that the thermal degradation of PVA may lead to the formation of aldehyde and alkene end molecules, and subsequently rearranged into vinyl ester molecules. Ultimately, the conversion stage from around 420 to 510 °C corresponds to the formation of polyaromatics. It is worth noting that the higher content of nanocellulose results in the shift toward higher conversion temperature, showing improved thermal stability.

The relative thermal stability is analyzed from the initial degradation of the composite, i.e, at 200–300 °C. As shown in Fig. 7(a), distinct shifts of initial degradation to higher temperature were observed for samples with higher amount of nanocellulose. Samples with 0 and 1 wt.% of nanocellulose start to degrade at around 250 °C. Meanwhile, samples with nanocellulose content > 1% initially degrade at temperature around 270 °C. Furthermore, the relative thermal stability is also described as T_{50}, the temperature when a half fraction of the samples has been converted (α = 0.5). The sample with a lower T_{50} exhibits better thermal stability. As seen

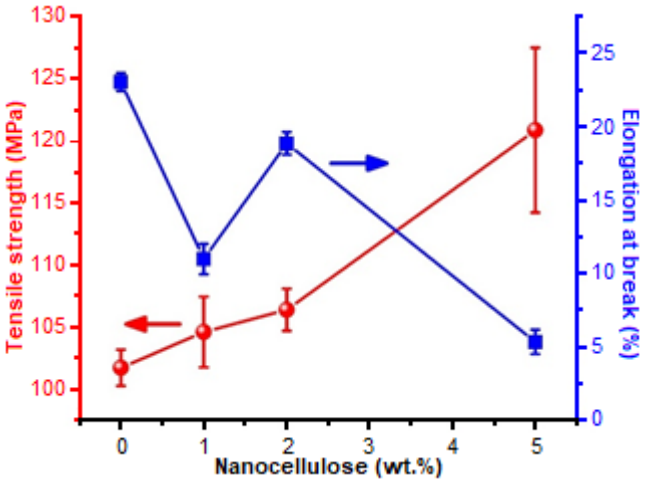

Fig 6. Mechanical properties of PVA-alginate composites with different amounts of nanocellulose addition

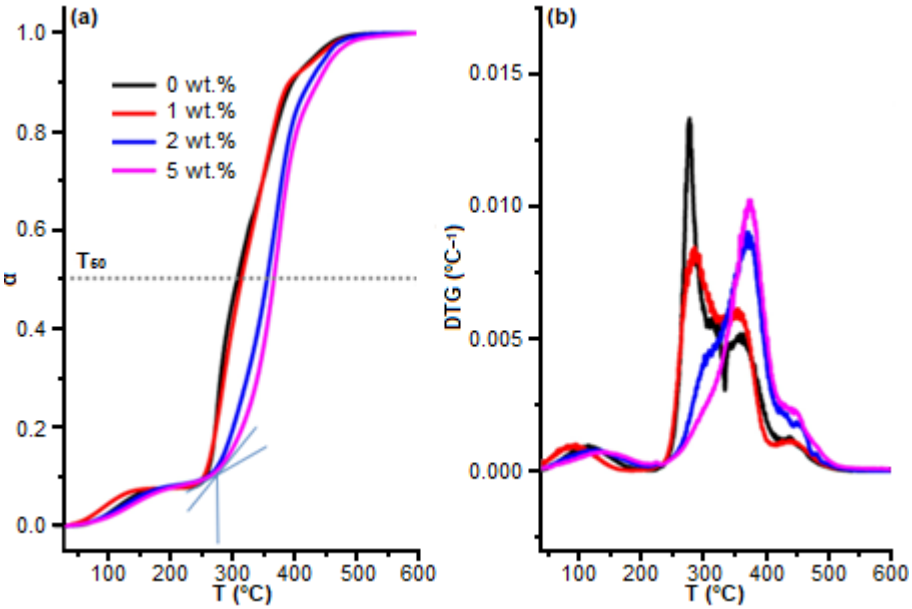

Fig 7. (a) TGA and (b) DTG curves of PVA-alginate composites with different amounts of nanocellulose addition

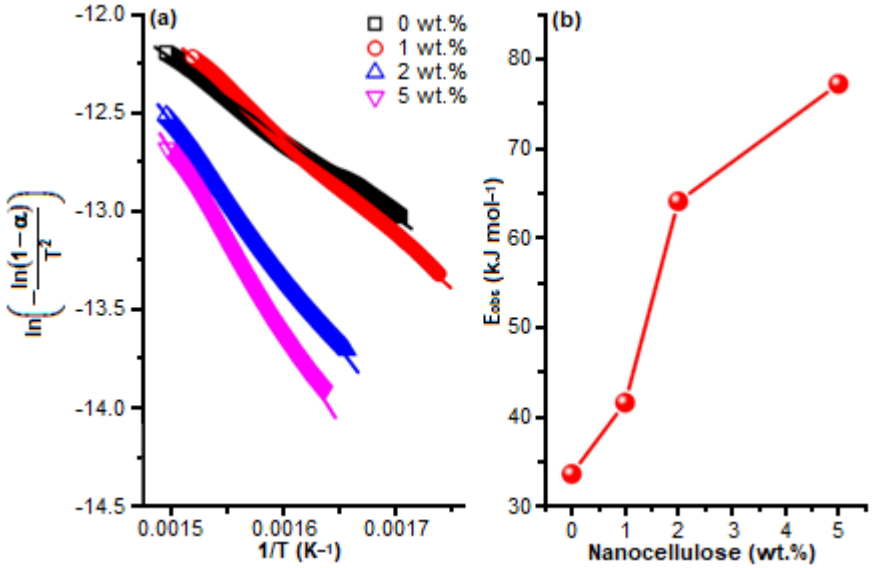

Fig 8. (a) Coats-Redfern plots and (b) E_{obs} of PVA-alginate composites with different amount of nanocellulose addition

in Fig. 7(a), the T_{50} shifts gradually to a higher value when a higher content of nanocellulose is added, based on the following order, 0 wt.% (308 °C) < 1 wt.% (315 °C) < 2 wt.% (355 °C) < 5 wt.% (367 °C). This result clearly demonstrates the usability of nanocellulose to reinforce the thermal stability of PVA-alginate composite yarn. The TGA curves can be further analyzed to determine the observed activation energy (E_{obs}) through the Coats-Redfern method since the thermal degradation of polymer is a first-order reaction. This model is a multi-heating rate that has been widely used for kinetic analysis of thermal decomposition [46-48]. Shukla et al. [49] also used this model for the multi-stage decomposition of epoxidized resole resin. This Coats-Redfern method is expressed as Eq. (2) [50-52],

$$\frac{da}{dT} = k(T)f(\alpha) = A\exp\left(-\frac{E_{obs}}{RT}\right)(1-\alpha) \quad (2)$$

where T is the temperature, A is the pre-exponential factor, and R is the ideal gas constant. Under the non-isothermal heating with a constant ramping, β = dT/dt,

Eq. (2) can be rearranged and integrated, resulting in the following equation,

$$\ln\left(-\frac{\ln(1-\alpha)}{T^2}\right)=\ln\left(\frac{AR}{\beta E_{obs}}\left(1-\frac{2RT}{E_{obs}}\right)\right)-\frac{E_{obs}}{RT} \quad (3)$$

Plotting $\ln\left(-\frac{\ln(1-\alpha)}{T^2}\right)$ against $\frac{1}{T}$ will result in a linear correlation with a slope of $-\frac{E_{obs}}{R}$ as shown in Fig. 8(a). Thus, the observed activation energy can be calculated by multiplying the slope with R (8.314 J mol^{-1} K^{-1}). The calculation results are provided in Fig. 8(b). It is clearly demonstrated that the composite with higher nanocellulose content possesses enhanced observed activation energy. This is possible since the presence of nanocellulose strengthens the interaction within the composite through hydrogen bonds; hence, greater energy consumption is necessary to thermally degrade the composite.

■ CONCLUSION

PVA-alginate composite yarns reinforced with nanocellulose isolated from OPEFBs were successfully prepared *via* a wet spinning method with improved mechanical and thermal properties. The isolated nanocellulose displays well compatibility as the nanofiller within PVA – alginate matrices. Moreover, the peculiar structure of nanocellulose with an abundant presence of hydroxyl groups enables more and strong hydrogen bonds with the functional groups of PVA and alginate, leading to more robust interfacial adhesion. The addition of nanocellulose, i.e., 1 wt.%, 2 wt.%, and 5 wt.% gives rise to the mechanical properties of PVA-alginate composite yarn from 101.7 MPa to 104.6 MPa, 106.4 MPa, and 120.1 MPa, respectively. On the other hand, the trend of elongation at break shows the opposite trend since the more and stronger hydrogen bond increases the composite stiffness. The same molecular interaction also takes responsibility for the higher energy consumption for the composite to undergo degradation. As the nanocellulose content increases, the initial stage degradation, T_{50}, and E_{obs} are enhanced, demonstrating the upgrading of the thermal stability. Our result shows that the nanocellulose isolated from OPEFBs possesses an up-and-coming potential as sustainable materials for effectively reinforcing the polymer composites.

■ ACKNOWLEDGMENTS

We acknowledge a collaborative RKI program from the Indonesian World Class University Research scheme.

■ REFERENCES

[1] Brad, A., Schaffartzik, A., Pichler, M., and Plank, C., 2015, Contested territorialization and biophysical expansion of oil palm plantations in Indonesia, *Geoforum*, 64, 100–111.

[2] Gatto, M., Wollni, M., and Qaim, M., 2015, Oil palm boom and land-use dynamics in Indonesia: The role of policies and socioeconomic factors, *Land Use Policy*, 46, 292–303.

[3] Varkkey, H., Tyson, A., and Choiruzzad, S.A.B., 2018, Palm oil intensification and expansion in Indonesia and Malaysia: Environmental and socio-political factors influencing policy, *For. Policy Econ.*, 92, 148–159.

[4] Kim, S., and Kim, C.H., 2013, Bioethanol production using the sequential acid/alkali-pretreated empty palm fruit bunch fiber, *Renewable Energy*, 54, 150–155.

[5] Alam, M.Z., Muyibi, S.A., Mansor, M.F., and Wahid, R., 2007, Activated carbons derived from oil palm empty-fruit bunches: Application to environmental problems, *J. Environ. Sci.*, 19 (1), 103–108.

[6] Osman, N.B., Shamsuddin, N., and Uemura, Y., 2016, Activated carbon of oil palm empty fruit bunch (EFB); Core and shaggy, *Procedia Eng.*, 148, 758–764.

[7] Ooi, C.H., Cheah, W.K., Sim, Y.L., Pung, S.Y., and Yeoh, F.Y., 2017, Conversion and characterization of activated carbon fiber derived from palm empty fruit bunch waste and its kinetic study on urea adsorption, *J. Environ. Manage.*, 197, 199–205.

[8] Loo, W.W., Pang, Y.L., Lim, S., Wong, K.H., Lai, C.W., and Abdullah, A.Z., 2021, Enhancement of photocatalytic degradation of malachite green using iron doped titanium dioxide loaded on oil palm empty fruit bunch-derived activated carbon, *Chemosphere*, 272, 129588.

[9] Derman, E., Abdulla, R., Marbawi, H., and Sabullah, M.K., 2018, Oil palm empty fruit bunches as a promising feedstock for bioethanol production in Malaysia, *Renewable Energy*, 129, 285–298.

[10] Sudiyani, Y., Styarini, D., Triwahyuni, E., Sudiyarmanto, Sembiring, K.C., Aristiawan, Y., Abimanyu, H., and Han, M.H., 2013, Utilization of biomass waste empty fruit bunch fiber of palm oil for bioethanol production using pilot–scale unit, *Energy Procedia*, 32, 31–38.

[11] Pangsang, N., Rattanapan, U., Thanapimmetha, A., Srinopphakhun, P., Liu, C.G., Zhao, X.Q., Bai, F.W., and Sakdaronnarong, C., 2019, Chemical-free fractionation of palm empty fruit bunch and palm fiber by hot-compressed water technique for ethanol production, *Energy Rep.*, 5, 337–348.

[12] Suhartini, S., Rohma, N.A., Mardawati, E., Kasbawati, Hidayat, N., and Melville, L., 2022, Biorefining of oil palm empty fruit bunches for bioethanol and xylitol production in Indonesia: A review, *Renewable Sustainable Energy Rev.*, 154, 111817.

[13] Lisdayana, N., Fahma, F., Sunarti, T.C., and Iriani, E.S., 2020, Thermoplastic starch-PVA nanocomposite films reinforced with nanocellulose from oil palm empty fruit bunches (OPEFBs): Effect of starch type, *J. Nat. Fibers*, 17 (7), 1069–1080.

[14] Huang, S., Zhao, Z., Feng, C., Mayes, E., and Yang, J., 2018, Nanocellulose reinforced P(AAm-*co*-AAc) hydrogels with improved mechanical properties and biocompatibility, *Composites, Part A*, 112, 395–404.

[15] Fahma, F., Lisdayana, N., Abidin, Z., Noviana, D., Sari, Y.W., Mukti, R.R., Yunus, M., Kusumaatmaja, A., and Kadja, G.T.M., 2019, Nanocellulose-based fibers derived from palm oil by-products and their in vitro biocompatibility analysis, *J. Text. Inst.*, 111 (9), 1354–1363.

[16] Septevani, A.A., Rifathin, A., Sari, A.A., Sampora, Y., Ariani, G.N., Sudiyarmanto, and Sondari, D., 2020, Oil palm empty fruit bunch-based nanocellulose as a super-adsorbent for water remediation, *Carbohydr. Polym.*, 229, 115433.

[17] Sawar, M.S., Niazi, M.B.K., Jahan, Z., Ahmad, T., and Hussain, A., 2018, Preparation and characterization of PVA/nanocellulose/Ag nanocomposite films for antimicrobial food packaging, *Carbohydr. Polym.*, 184, 453–464.

[18] Jorfi, M., and Foster, E.J., 2015, Recent advances in nanocellulose for biomedical applications, *J. Appl. Polym. Sci.*, 132 (14), 41719.

[19] Salimi, S., Sotudeh-Gharebagh, R., Zargami, R., Chan, S.Y., and Yuen, K.H., 2019, Production of nanocellulose and its applications in drug delivery: A critical review, *ACS Sustainable Chem. Eng.*, 7 (19), 15800–15827.

[20] Liu, J., Chinga-Carrasco, G., Cheng, F., Xu, W., Willför, S., Syverud, K., and Xu, C., 2016, Hemicellulose-reinforced nanocellulose hydrogels for wound healing application, *Cellulose*, 23, 3129–3143.

[21] Basu, A., Lindh, J., Ålander, E., Strømme, M., and Ferraz, N., 2017, On the use of ion-crosslinked nanocellulose hydrogels for wound healing solutions: Physicochemical properties and application-oriented biocompatibility studies, *Carbohydr. Polym.*, 174, 299–308.

[22] Savadekar, N.R., and Mhaske, S.T., 2012, Synthesis of nano cellulose fibers and effect on thermoplastics starch based films, *Carbohydr. Polym.*, 89 (1), 146–151.

[23] Cataldi, A., Rigotti, D., Nguyen, V.D.H., and Pegoretti, A., 2018, Polyvinyl alcohol reinforced with crystalline nanocellulose for 3D printing application, *Mater. Today Commun.*, 15, 236–244.

[24] Chen, C., Wang, H., Li, S., Fang, L., and Li, D., 2017, Reinforcement of cellulose nanofibers in polyacrylamide gels, *Cellulose*, 24 (12), 5487–5493.

[25] Khalil, H.P.S.A., Saurabh, C.K., Adnan, A.S., Nurul Fazita, M.R., Syakir, M.I., Davoudpour, Y., Rafatullah, M., Abdullah, C.K., Haafiz, M.K.M., and Dungani, R., 2016, A review on chitosan-cellulose blends and nanocellulose reinforced chitosan biocomposites: Properties and their applications, *Carbohydr. Polym.*, 150, 216–226.

[26] Abdollahi, M., Alboofetileh, M., Rezaei, M., and Behrooz, R., 2013, Comparing physico-mechanical and thermal properties of alginate nanocomposite

films reinforced with organic and/or inorganic nanofillers, *Food Hydrocolloids*, 32 (2), 416–424.

[27] Poonguzhali, R., Basha, S.K., and Kumari, V.S., 2017, Synthesis and characterization of chitosan-PVP-nanocellulose composites for in-vitro wound dressing application, *Int. J. Biol. Macromol.*, 105, 111–120.

[28] Mandal, A., and Chakrabarty, D., 2015, Characterization of nanocellulose reinforced semi-interpenetrating polymer network of poly(vinyl alcohol) & polyacrylamide composite films, *Carbohydr. Polym.*, 134, 240–250.

[29] Li, W., Wu, Q., Zhao, X., Huang, Z., Cao, J., Li, J., and Liu, S., 2014, Enhanced thermal and mechanical properties of PVA composites formed with filamentous nanocellulose fibrils, *Carbohydr. Polym.*, 113, 403–410.

[30] Jiang, X., Xiang, N., Zhang, H., Sun, Y., Lin, Z., and Hou, L., 2018, Preparation and characterization of poly(vinyl alcohol)/sodium alginate hydrogel with high toughness and electric conductivity, *Carbohydr. Polym.*, 186, 377–383.

[31] Islam, M.S., and Karim, M.R., 2010, Fabrication and characterization of poly(vinyl alcohol)/alginate blend nanofibers by electrospinning method, *Colloids Surf., A*, 366 (1-3), 135–140.

[32] Fahma, F., Sapoan, M., Lisdayana, N., Iskandar, A., Sunarti, T.C., and Sugiarto, 2021, Release property of red ginger essential oil in silica-nanocellulose composite based sachet, *IOP Conf. Ser.: Earth Environ. Sci.*, 749, 012045.

[33] Zuluaga, R., Putaux, J.L., Restrepo, A., Mondragon, I., and Gañán, P., 2007, Cellulose microfibrils from banana farming residues: Isolation and characterization, *Cellulose*, 14, 585–592.

[34] Wang, Q., Hu, X., Du, Y., and Kennedy, J.F., 2010, Alginate/starch blend fibers and their properties for drug controlled release, *Carbohydr. Polym.*, 82 (3), 842–847.

[35] French, A.D., and Cintrón, M.S., 2013, Cellulose polymorphy, crystallite size, and the Segal crystallinity index, *Cellulose*, 20 (1), 583–588.

[36] Zhao, Y., Moser, C., Lindström, M.E., Henriksson, G., and Li, J., 2017, Cellulose nanofibers from softwood, hardwood, and tunicate: Preparation-structure-film performance interrelation, *ACS Appl. Mater. Interfaces*, 9 (15), 13508–13519.

[37] Uddin, A.J., Araki, J., and Gotoh, Y, 2011, Toward "strong" green nanocomposites: Polyvinyl alcohol reinforced with extremely oriented cellulose whiskers, *Biomacromolecules*, 12 (3), 617–624.

[38] Peng, J., Ellingham, T., Sabo, R., Turng, L.S., and Clemons, C.M., 2014, Short cellulose nanofibrils as reinforcement in polyvinyl alcohol fiber, *Cellulose*, 21 (6), 4287–4298.

[39] Yue, Y., Han, J., Han, G., French, A.D., Qi, Y., and Wu, Q., 2016, Cellulose nanofibers reinforced sodium alginate-polyvinyl alcohol hydrogels: Core-shell structure formation and property characterization, *Carbohydr. Polym.*, 147, 155–164.

[40] Rozenberg, M., Loewenschuss, A., and Marcus, Y., 2000, An empirical correlation between stretching vibration redshift and hydrogen bond length, *Phys. Chem. Chem. Phys.*, 2 (12), 2699–2702.

[41] Joseph, J., and Jemmis, E.D., 2007, Red-, Blue-, or No-shift in hydrogen bond: A unified explained, *J. Am. Chem. Soc.*, 129 (15), 4620–4632.

[42] Li, X., Shu, M., Li, H., Gao, X., Long, S., Hu, T., and Wu, C., 2018, Strong, tough and mechanically self-recoverable poly(vinyl alcohol)/alginate dual-physical double-network hydrogels with large cross-link density contrast, *RSC Adv.*, 8 (30), 16674–16689.

[43] Cho, M.J., and Park, B.D., 2011, Tensile and thermal properties of nanocellulose-reinforced poly(vinyl alcohol) nanocomposites, *J. Ind. Eng. Chem.*, 17 (1), 36–40.

[44] El Miri, N., Abdelouahdi, K., Barakat, A., Zahouily, M., Fihri, A., Solhy, A., and El Achaby, M., 2015, Bio-nanocomposite films reinforced with cellulose nanocrystals: Rheology of film-forming solutions, transparency, water vapor barrier and tensile properties of films, *Carbohydr. Polym.*, 129, 156–167.

[45] Holland, B.J., and Hay, J.N., 2001, The thermal degradation of poly(vinyl alcohol), *Polymer*, 42 (16), 6775–6783.

[46] Al-Bayaty, S.A., Al-Uqaily, R.A.H., and Jubier, N.J., 2020, Using the Coats-Redfern method during thermogravimetric analysis and differential scanning calorimetry analysis of the thermal stability of epoxy and epoxy/silica nanoparticle nanocomposites, *J. Southwest Jiaotong Univ.*, 55 (4), 1–12.

[47] Cai, J., and Bi, L., 2008, Precision of the Coats and Redfern method for the determination of the activation energy without neglecting the low-temperature end of the temperature integral, *Energy Fuels*, 22 (4), 2172–2174.

[48] Ge, J., Wang, R.Q., and Liu, L., 2016, Study on the thermal degradation kinetics of the common wooden boards, *Procedia Eng.*, 135, 72–82.

[49] Shukla, S.K., Srivastava, D., and Srivastava, K., 2015, Synthesis, spectral and thermal degradation kinetics of the epoxidized resole resin derived from cardanol, *Adv. Polym. Technol.*, 34 (1), 21469.

[50] Huang, S., Zhou, L., Li, M.C., Wu, Q., and Zhou, D., 2017, Cellulose nanocrystals (CNCs) from corn stalk: Activation energy analysis, *Materials*, 10 (1), 80.

[51] Wardani, M.K., Kadja, G.T.M., Fajar, A.T.N., Subagjo, Makertihartha, I.G.B.N., Gunawan, M.L., Suendo, V., and Mukti, R.R., 2019, Highly crystalline mesoporous SSZ-13 zeolite obtained *via* controlled post-synthetic treatment, *RSC Adv.*, 9 (1), 77–86.

[52] Kadja, G.T.M., Suprianti, T.R., Ilmi, M.M., Khalil, M., Mukti, R.R., and Subagjo, 2020, Sequential mechanochemical and recrystallization methods for synthesizing hierarchically porous ZSM-5 zeolites, *Microporous Mesoporous Mater.*, 308, 110550.